

Article

“Low Cost” Pore Expanded SBA-15 Functionalized with Amine Groups Applied to CO₂ Adsorption

Enrique Vilarrasa-García ^{1,2}, Juan Antonio Cecilia ², Elisa Maria Ortigosa Moya ², Celio Loureiro Cavalcante, Jr. ¹, Diana Cristina Silva Azevedo ¹ and Enrique Rodríguez-Castellón ^{2,*}

¹ Department of Chemical Engineering, Universidade Federal do Ceará, Campus do Pici, bl. 709, 60455-760 Fortaleza, Brazil; E-Mails: evilarrasa@uma.es (E.V.-G.); celio@gpsa.ufc.br (C.L.C.); diana@gpsa.ufc.br (D.C.S.A.)

² Departament of Inorganic Chemistry, Crystallography and Mineralogy, Universidad de Málaga, Campus de Teatinos s/n, 29071 Málaga, Spain; E-Mails: jacecilia@uma.es (J.A.C.); 061776459x@uma.es (E.M.O.M.)

* Author to whom correspondence should be addressed; E-Mail: castellon@uma.es; Tel.: +34-952-131873.

Academic Editor: Rafael Luque

Received: 1 March 2015 / Accepted: 30 April 2015 / Published: 11 May 2015

Abstract: The CO₂ adsorption capacity of different functionalized mesoporous silicas of the SBA-15 type was investigated and the influence of textural properties and the effect of the silicon source on the CO₂ uptake studied. Several adsorbents based on SBA-15 were synthesized using sodium silicate as silicon source, replacing the commonly used tetraethyl orthosilicate (TEOS). Thus, we synthesized three couples of supports, two at room temperature (RT, RT-F), two hydrothermal (HT, HT-F) and two hydrothermal with addition of swelling agent (1,3,5-triisopropylbenzene) (TiPB, TiPB-F). Within each couple, one of the materials was synthesized with ammonium fluoride (NH₄F). The supports were functionalized via grafting 3-aminopropyltriethoxysilane (APTES) and via impregnation with polyethylenimine ethylenediamine branched (PEI). The adsorption behavior of the pure materials was described well by the Langmuir model, whereas for the amine-silicas, a Dualsite Langmuir model was applied, which allowed us to qualify and quantify two different adsorption sites. Among the materials synthesized, only the SBA-15 synthesized at room temperatures (RT) improved its properties as an adsorbent with the addition of

fluoride when the silicas were functionalized with APTES. The most promising result was the TiPB-F/50PEI silica which at 75 °C and 1 bar CO₂ captured 2.21 mmol/g.

Keywords: SBA-15; 1,3,5-triisopropylbenzene; ammonium fluoride; adsorption; CO₂; 3-aminopropyltriethoxysilane; polyethylenimine ethylenediamine; Dualsite Langmuir model; chemisorptions

1. Introduction

Since the beginning of the industrialization era, the emissions of greenhouse gases such as carbon dioxide (CO₂), methane (CH₄), nitrous oxide (N₂O), chlorofluorocarbons (CFC), and sulfur hexafluoride (SF₆) have been continuously increasing. Thus, the average world temperature has increased by 0.74% in the past 100 years and is expected to increase by another 6.4% by the end of the twenty-first century [1]. The emissions of greenhouse gases cause the global warming, which is directly related with droughts, floods, heat waves, and destruction of ecosystems [2]. This fact has led to more restrictive environmental requirements by governments to reduce CO₂ emissions to the atmosphere.

Among the currently available technologies, post-combustion capture, a technology for capturing CO₂ from post-combustion emission gases, is the most easily applied technology for existing emission sources. Post-combustion capture uses wet/dry adsorbents, which are used for gas separation, and separates and collects CO₂ by adsorption/desorption. In general, post-combustion capture technologies include wet absorption, dry adsorption, membrane-based technologies, and cryogenics [3,4].

Wet absorption is good for treating large emission volumes from combustion, however, it demands high energy for absorbent regeneration, suffers from loss of effectiveness over time due to low solvent thermal stability, and usually requires a large footprint. In addition, this technology has some drawbacks such as high equipment corrosion rate and losses due to solvent evaporation [5,6]. Membrane-based processes generally require simple devices, are easy to operate, and have low energy consumption. However, they entail high-cost membrane modules, which are not suitable for treating large volumes of emission gases and may suffer from fast fouling [7,8]. Cryogenics requires low investment cost and it is a mature technology; however, it is not suitable in most cases because of its energy consumption. Current research is focused on dry adsorption systems using dry adsorbents. This technology requires simple devices, which are robust and easy to operate [9]. Nevertheless, the choice of an adsorbent with a suitable working capacity, selectivity, and regenerability is still an open issue.

The process of capturing CO₂ using a dry adsorbent involves selective separation of CO₂ based on gas-solid interactions, using molecular sieves such as zeolites [10–12], activated carbons [13,14], metal-organic frameworks (MOF) [15,16] and porous silica such as SBA-15 [17–25], MCM-41 [21,26–28] and mesocellular foams (MCF) [22,24,25,29,30]. The synthesis of both SBA-15 and MCM-41 requires surfactant templates in order to give rise to ordered mesoporous materials. Note that the polymer employed to obtain SBA-15, poly(ethylene oxide)–poly(propylene oxide)–poly(ethylene oxide) (PEO–PPO–PEO), is biodegradable and cheaper than the surfactants used initially in the synthesis of MCM-41 [31]. In addition, a feature of SBA-15 is the interconnection between channels that facilitate diffusion inside the entire porous structure and may pose a significant contribution in gas

physisorption [32]. In the last decade, many efforts have focused on the modification of SBA-15 to more effectively tailor it for its application as catalyst or adsorbent.

Thus, the pore size of SBA-15 can be increased by the incorporation of swelling agents such as aromatics compounds [24,25] or alkanes [24], which favors the diffusion of bulky molecules. The presence of fluoride species in the synthesis conditions limits the aggregation and growth of the mesochannels and disrupts the honeycomb arrangement of SBA-15, leading to spherical cells that are interconnected by windows with a narrow pore size distribution [24,25,33]. An important issue related to the potential applications of the ordered mesoporous materials, such as SBA-15 or MCM-41, is their large scale synthesis, which needs to be simple and economically feasible. Alkoxides, such as tetraethyl orthosilicate (TEOS), are a quite expensive silica source, which should be replaced by a less costly and more environmentally friendly silica compound. Stucky *et al.* [34] reported a slightly modified synthesis of SBA-15 using an inexpensive sodium metasilicate as silicon source, obtaining materials with similar behavior as those prepared with TEOS.

The incorporation of amine species (by impregnation or grafting) produces a significant increase in the CO₂ adsorption capacity. In the case of the impregnation method, large amounts of amine polymers are stabilized inside the porous framework by electrostatic interactions between the amine groups and the silanol species of the porous silica based material [17,24,25,30]. Nonetheless, bulky amine polymers may detrimentally affect CO₂ adsorption by clogging the porous matrix [35]. The grafting method takes place by reacting an aminosilane the silanol species present on the solid surface, leading to amine modified porous silica. Such grafted silicas have been reported to have high stability and outstanding CO₂ capacity [20,24,25].

The aim of this work was the synthesis and characterization of SBA-15 using a low cost and environmentally friendly source such as sodium metasilicate. The uniqueness of this study is based on the modification of low-cost SBA-15 with the use of a swelling agent such as 1,3,5-triisopropylbenzene, which increases the pore size and/or the addition of fluoride, which limits the growing of mesochannels of the porous framework, diminishing the diffusion problems. In both cases the textural properties of the low-cost SBA-15 are strongly modified. The porous silica materials were either grafted with 3-(triethoxysilyl)propylamine (APTES) or impregnated with polyethyleneimine (PEI) to be tested for CO₂ capture.

2. Experimental

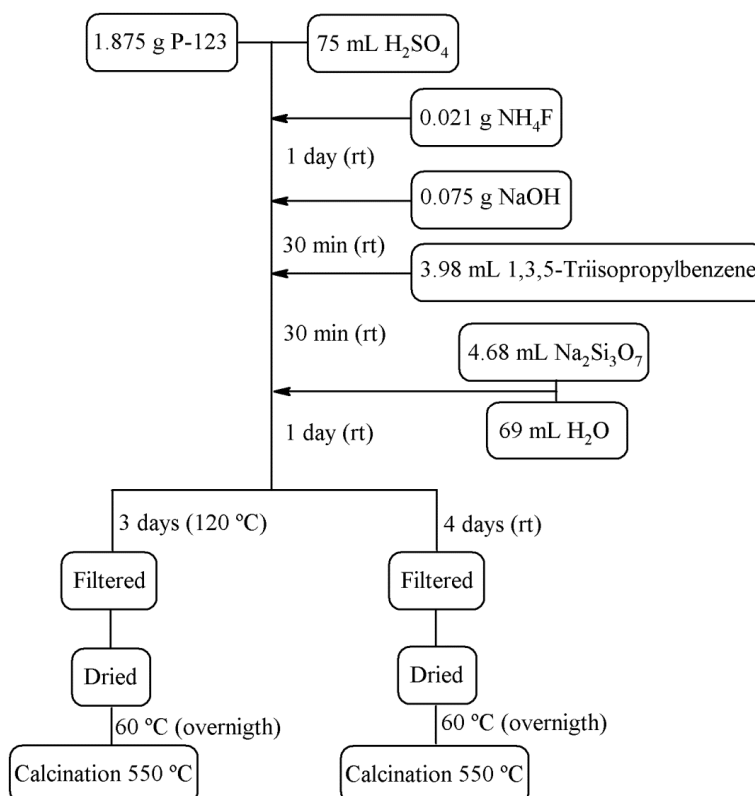
2.1. Materials

The chemicals used to synthesize the various mesoporous silica samples by soft templating were triblock copolymers Pluronic P123 (PEO₂₀PPO₇₀PEO₂₀ average molecular weight $M_n = 5800 \text{ g mol}^{-1}$, Aldrich, St. Louis, MO, USA), sodium silicate solution (Na₂Si₃O₇ with 27% SiO₂ and 14% NaOH from Aldrich), sodium hydroxide (NaOH, Prolabo, PA, USA) and sulfuric acid (H₂SO₄, VWR 95%). In order to enlarge the pore volume and shorten the length of the channels, 1,3,5-triisopropylbenzene (Aldrich 95%) and NH₄F (Aldrich) were employed, respectively. The functionalization of the thus synthesized silicas was performed with branched polyethylenimine ethylenediamine (PEI) (average molecular weight $M_n \sim 600$, Aldrich) and 3-aminopropyltriethoxysilane (APTES) (Aldrich 98%), using

methanol (Aldrich 99.9%) and toluene (Aldrich 99.5%) as solvents, respectively. The gases employed in this work were He (Air Liquide, Paris, France, 99.99%), N₂ (Air Liquide 99.9999%) and CO₂ (Air Liquide 99.998%).

2.2. Preparation of Siliceous Porous Structures

The synthesis of the low-cost porous silica was obtained following the synthesis reported by Gómez-Cazalilla *et al.* [36] with modifications by the use of a swelling agent such as 1,3,5-triisopropylbenzene or/and NH₄F to reduce the length of the channels. The synthetic conditions and final molar ratio in the synthesis gel are summarized in Scheme 1 and Table 1.



Scheme 1. Synthesis of pure silicas.

Table 1. Final molar composition of the synthesis gel.

Sample	Description	P123/SiO ₂ /H ₂ SO ₄ /NaOH/NH ₄ F/TIPB/H ₂ O
RT	Room temperature SBA15	1/189/93/5.8/0/0/4447
RT-F	Room temperature porous silica modified with fluoride	1/189/93/5.8/1.7/0/4447
HT	Hydrothermal SBA15	1/189/93/5.8/0/0/4447
HT-F	Hydrothermal porous silica modified with fluoride	1/189/93/5.8/1.7/0/4447
TiPB	Hydrothermal SBA-15 modified with pore expander (TiPB)	1/189/93/5.8/0/49/4447
TiPB-F	Hydrothermal porous silica modified with pore expander (TIPB)	1/189/93/5.8/1.7/49/4447

In a typical synthesis, 1.875 g Pluronic was added to 75 mL H₂SO₄ 0.4 M solution. After stirring for a few hours, a clear solution was obtained. Then, 0.075 g NaOH and 4.68 mL sodium silicate solution were added at room temperature under magnetic stirring. The resulting gel mixture was stirred for 5 days at room temperature, the final pH was about 1. The solid product was recovered by filtration, washed several times with water, and dried overnight at 60 °C.

All materials were calcined at a heating rate of 1 °C min⁻¹ to 550 °C and maintained at this temperature for 6 h. The mesoporous materials were labeled as indicated in Table 1.

2.3. Characterization Techniques

X-ray diffraction (XRD) was used to identify the crystalline phases of the synthesized solids. These experiments were performed on an X'Pert Pro MPD automated diffractometer (PANalytical, Almelo, The Netherlands) equipped with a Ge (111) primary monochromator (strictly monochromatic Cu-K α radiation) and an X'Celerator detector. Measurements were obtained for 2 h in the range of 1°–10°.

The textural parameters (S_{BET} , V_{P} and D_{P}) were evaluated from nitrogen adsorption–desorption isotherms at –196 °C as determined by an automatic ASAP 2020 system from Micromeritics. Prior to the measurements, samples were degassed at 200 °C and 10⁻⁴ mbar overnight. Surface areas were determined by using the Brunauer–Emmett–Teller (BET) equation assuming a cross section of 16.2 Å² for the nitrogen molecule. Micropore surface areas were obtained by de Boer's t-plot method [37] for relative pressures between 0.35 and 0.70. The pore size distribution was calculated by applying the Barrett–Joyner–Halenda (BJH) method applied to the desorption branch of the N₂ isotherm. The total pore volume was calculated from adsorbed N₂ at $P/P_0 = 0.996$.

FTIR spectra were collected on a Varian 3100 FTIR spectrophotometer (Varian Inc., Walnut Creek, CA, USA). The interferograms consisted of 200 scans, and the spectra were collected using a KBr spectrum as background. About 30 mg of a mixture of each sample and KBr at a weight ratio of 1:9 were placed in the sample holder and then spectra were collected.

Elemental chemical analysis was performed with a LECO CHNS 932 analyzer (LECO Corporation, St. Joseph, MI, USA) to determine the nitrogen content present through the combustion of the samples at 1100 °C in pure oxygen to form NO.

Thermal analysis was performed on a TG-DTG thermobalance (Mettler Toledo, Columbus, OH, USA) with a continuous heating rate of 5 °C min⁻¹ in a helium flow.

2.4. CO₂ Adsorption Tests

CO₂ adsorption isotherms were measured with a Micromeritics ASAP 2020 Analyzer (Micromeritics Corp., Norcross, GA, USA) (*i.e.*, volumetrically) at 25 °C. Prior to the measurements, samples were degassed at 115 °C and 10⁻⁴ mbar overnight.

3. Results and Discussion

3.1. Characterization

The low-angle XRD diffractograms of the synthesized samples are depicted in Figure 1. Samples RT, RT-F, HT and HT-F (samples are labeled as indicated in Table 1) clearly show the (100)

reflection, which is associated to the P6mm hexagonal arrangement [38]. Although the addition to fluoride limits the length of the mesochannels, there is a shift of the (100) reflection towards lower values, which suggests an increase of the pore size in the hexagonal framework in all cases. The hydrothermal treatment leads to a shift to even lower $2\theta(^{\circ})$ values, revealing the formation of better ordered hexagonal materials with a larger pore size.

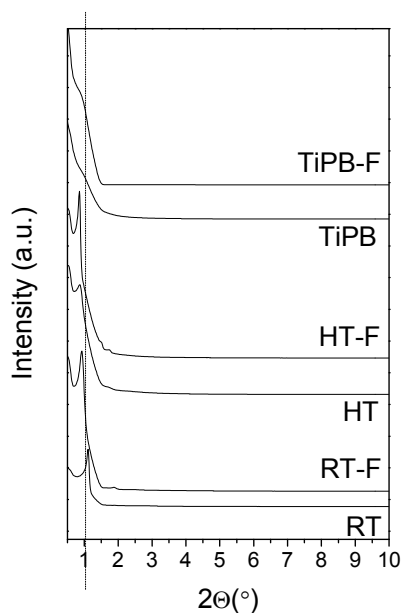


Figure 1. Low angle X-ray diffraction (XRD) patterns of pure silicas.

The addition of a swelling agent, such as 1,3,5-triisopropylbenzene, leads to a shift of the (100) reflection to lower angles, which has been attributed to the incorporation of swelling agents such as alkanes or derived benzene compounds that penetrate into the hydrophobic core of the surfactant micelle of P-123, disrupting the honeycomb packing typical of the hydrothermal SBA-15, leading to node separation into spherical micelles [39,40].

Figure 2 shows the nitrogen adsorption/desorption isotherms of the porous silicas. Samples without fluoride (RT, HT and TiPB) exhibit the classic type IV isotherms with parallel H1 type hysteresis loops. The hysteresis loop, which accounts for capillary condensation, is shifted toward higher P/P_0 when a swelling agent is added (TiPB). This fact is related to the larger pore sizes by the addition of 1,3,5-triisopropylbenzene, which is known to widen the hydrophobic core of the surfactant that shapes the pores of the silica.

The addition of ammonium fluoride also causes a shift of hysteresis loop to higher relative pressure together with a decrease in surface area, except for RT and RT-F samples, in which case the surface area increases with the addition of the fluoride salt (Table 2). This fact suggests that the temperature synthesis could have an influence on the behavior of samples. (RT and RT-F were synthesized at 25 °C).

Table 2 summarizes the textural properties of pure silicas. Note that the less ordered materials present lower surface areas but exhibit higher pore volumes. The addition of swelling agent produced the desired effect, leading to pore expanded materials (7.9 and 13.2 nm for TiPB and TiPB-F, respectively). Micropore volume and micropore surface area were higher for more ordered materials. In these materials, the micropores are formed due to the hydrophilic character of the ethylene oxide

chains, which remain trapped within the siliceous walls during the condensation step and leave interconnecting micropores upon surfactant removal by calcinations or solvent extraction [32,41–44].

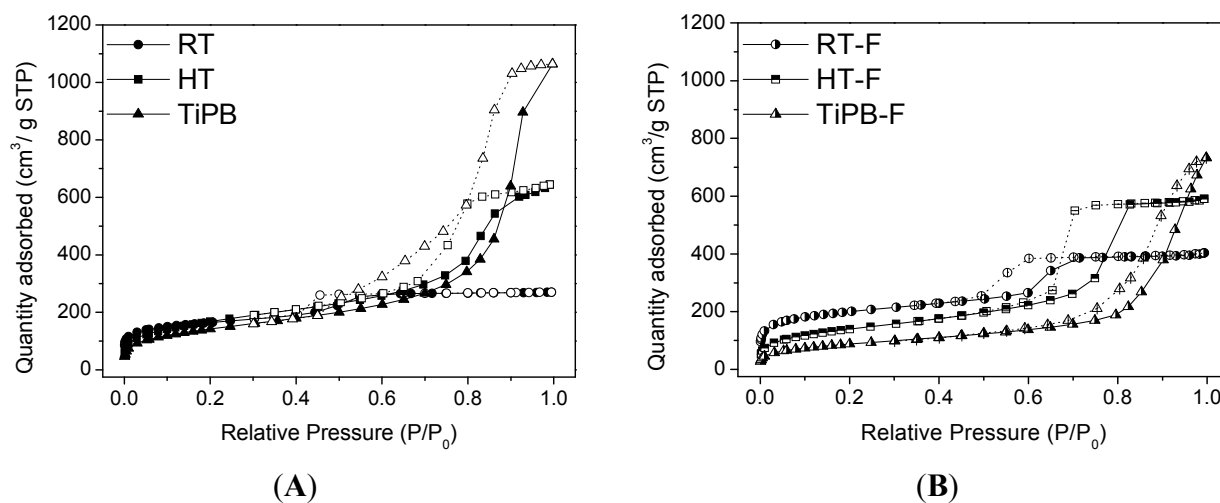


Figure 2. Nitrogen adsorption/desorption isotherms at $-196\text{ }^{\circ}\text{C}$ of pure silicas: (A) without fluoride (B) with fluoride.

Table 2. Textural properties of pure silicas.

Sample	S_{BET} (m^2/g)	$S_{\text{mp t-plot}}$ (m^2/g)	V_{P} (cm^3/g)	$V_{\text{mp t-plot}}$ (cm^3/g)	D_{P} (nm)
RT	571	256	0.42	0.12	3.6
RT-F	699	385	0.62	0.17	4.6
HT	613	148	0.99	0.06	7.5
HT-F	508	74	0.91	0.03	6.3
TiPB	519	74	1.64	0.02	7.9
TiPB-F	321	75	1.13	0.02	13.2

Notes: S_{BET} : equivalent surface area, as determined by Brunauer-Emmett-Teller equation; $S_{\text{mp t-plot}}/V_{\text{mp t-plot}}$: micropore surface area/micropore volume area, as determined by t-plot method; V_{P} : total pore volume, as calculated from adsorbed N_2 at $P/P_0 = 0.996$ ($-196\text{ }^{\circ}\text{C}$); D_{P} : pore diameter, as calculated by Barret-Joyner-Halenda (BJH) method to the desorption branch of the N_2 isotherm at $-196\text{ }^{\circ}\text{C}$.

The FTIR spectra for the different synthesized pure silicas and their respective amine functionalized counterparts are shown in Figure 3. The FTIR spectra of pure silicas (Figure 3A) show a narrow and intense band around 3700 cm^{-1} and a broad low frequency band centered at 3400 cm^{-1} . A first band is related to the symmetrical stretching vibration mode of isolated O-H in terminal silanol groups [45] and the broad band centered at 3400 cm^{-1} is due to those silanol groups with cross hydrogen bonding interactions with adsorbed water molecules [20,27,46–48]. The above mentioned band at around 3700 cm^{-1} has a major importance to ensure high grafting efficiency of the amine groups.

The spectra of amine silicas (Figure 3B,C) reveal the presence of two bands at 2950 and 2840 cm^{-1} assigned to C-H asymmetric and symmetric stretching modes of the APTES and PEI chains, respectively [49]. Furthermore, the bands located at 1565 and 1485 cm^{-1} are attributed to asymmetric and symmetric bending of primary amines ($-\text{NH}_2$) [25,50]. The presence of two bands around 3300 cm^{-1} is noticeable and may be assigned to N-H stretching vibrations [25], which provides evidence for the successful APTES grafting of the porous silicas [51,52]. Finally, the intensity of the band mentioned

above, at around 3700 cm^{-1} , decreases or is not observed in the FTIR spectra of amine functionalized silicas. This suggests that surface silanol groups have reacted with ethoxy groups from the aminosilane, thus providing evidence of the incorporation of organic molecules in the porous silica materials.

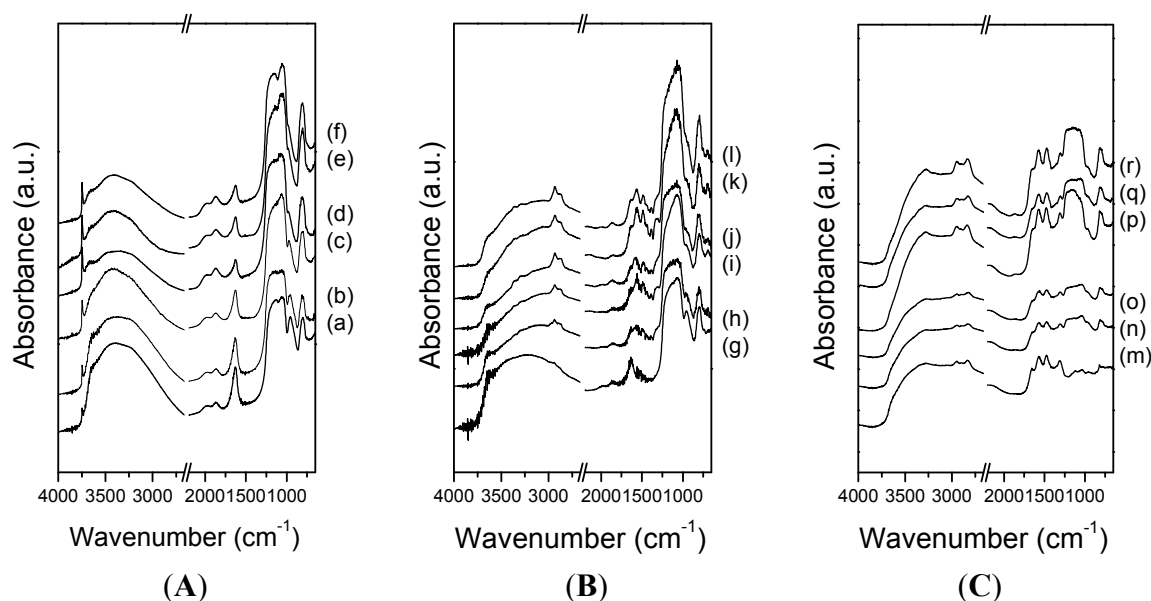


Figure 3. FTIR spectra of (A) pure silicas; (B) amine grafted silicas and (C) amine impregnated silicas (a) RT; (b) RT-F; (c) HT, (d) HT-F; (e) TiPB, (f) TiPB-F; (g) RT/20A, (h) RT-F/20A; (i) HT/20A; (j) HT-F/20A; (k) TiPB/20A; (l) TiPB-F/20A; (m) RT/50P; (n) RT-F/50P; (o) HT/50P; (p) HT-F/50P; (q) TiPB/50P and (r) TiPB-F/50P.

It is noteworthy that the band located at 1054 cm^{-1} related to Si-O-Si asymmetric stretching with a shoulder at 1160 cm^{-1} appears with a strong intensity in the amine grafted silicas (Figure 3B) whereas it is weaker in the more ordered impregnated silicas, perhaps due to the deposition of PEI layers that prevents a clean visualization of these bands.

3.2. CO₂ Adsorption

Figure 4 shows CO₂ adsorption /desorption isotherms on pure silicas obtained with sodium silicate solution. For non-functionalized supports, adsorption isotherms are virtually linear, thereby all isotherms show a gradual increase in the amount of the adsorbed CO₂ with an increase of pressure. Except for the samples synthesized at room temperature (RT and RT-F), all silicas adsorbed CO₂ at less than 0.6 mmol/g.

Experimental data were fit to the Langmuir adsorption model. More ordered pure silicas exhibit higher CO₂ capacities and also higher affinity to CO₂ capture (q and K values, Table 3). These results can be associated with the larger microporous network (less ordered materials present lower k values). The isotherms showed a nearly linear behavior, suggesting weak adsorbent–adsorbate affinity.

In Figure 5, CO₂ adsorption/desorption isotherms at 25 °C on amine-grafted silicas are plotted. All isotherms present hysteresis, due to strong interactions between CO₂ and amine groups, leading to incomplete desorption by only decreasing pressure. Note that special care was taken in these

experiments to allow for enough time for equilibrium to be reached, so that the hypothesis of diffusional resistances in the adsorption branch as a cause of this hysteresis could be ruled out.

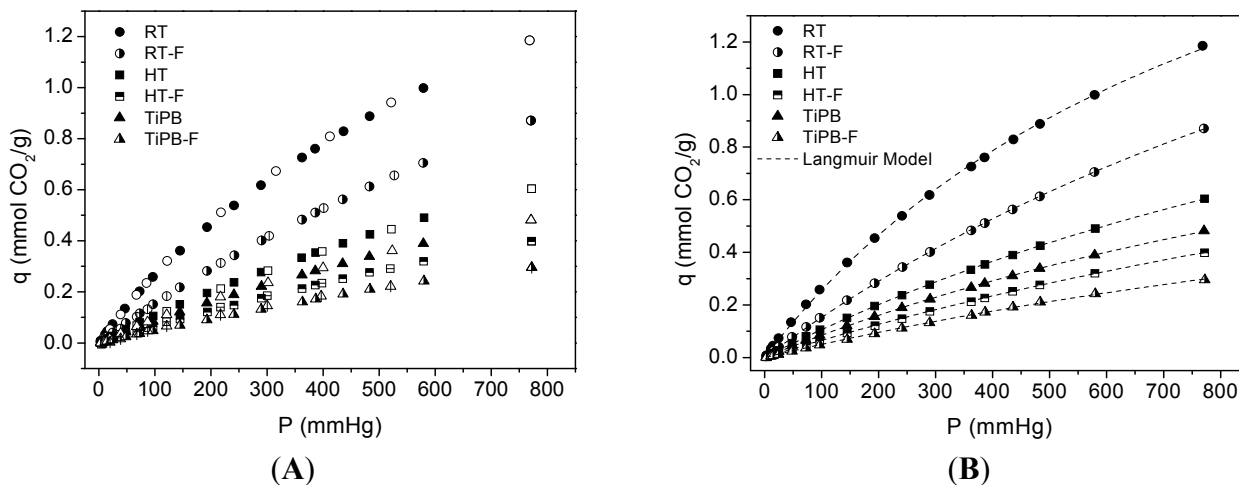


Figure 4. (A) CO₂ adsorption/desorption isotherms at 25 °C on pure silicas. Filled symbols stand for adsorption data and empty symbols stand for desorption data; dotted lines (B) are fits from the Langmuir model equation using adsorption data.

Table 3. Parameters from fit to Langmuir model for pure silicas.

Sample	Langmuir Model		q (25 °C, 1 bar)
	q (mmol CO ₂ /g)	K (mmHg ⁻¹)	
RT	2.53 ± 0.05	0.0011 ± 3.4 × 10 ⁻⁴	1.19
RT-F	2.88 ± 0.04	5.61 × 10 ⁻⁴ ± 1.03 × 10 ⁻⁵	0.87
HT	1.99 ± 0.03	5.59 × 10 ⁻⁴ ± 1.23 × 10 ⁻⁵	0.61
HT-F	1.69 ± 0.04	4.08 × 10 ⁻⁴ ± 1.06 × 10 ⁻⁵	0.39
TiPB	1.58 ± 0.03	5.66 × 10 ⁻⁴ ± 1.59 × 10 ⁻⁵	0.48
TiPB-F	1.16 ± 0.06	4.47 × 10 ⁻⁴ ± 2.73 × 10 ⁻⁵	0.29

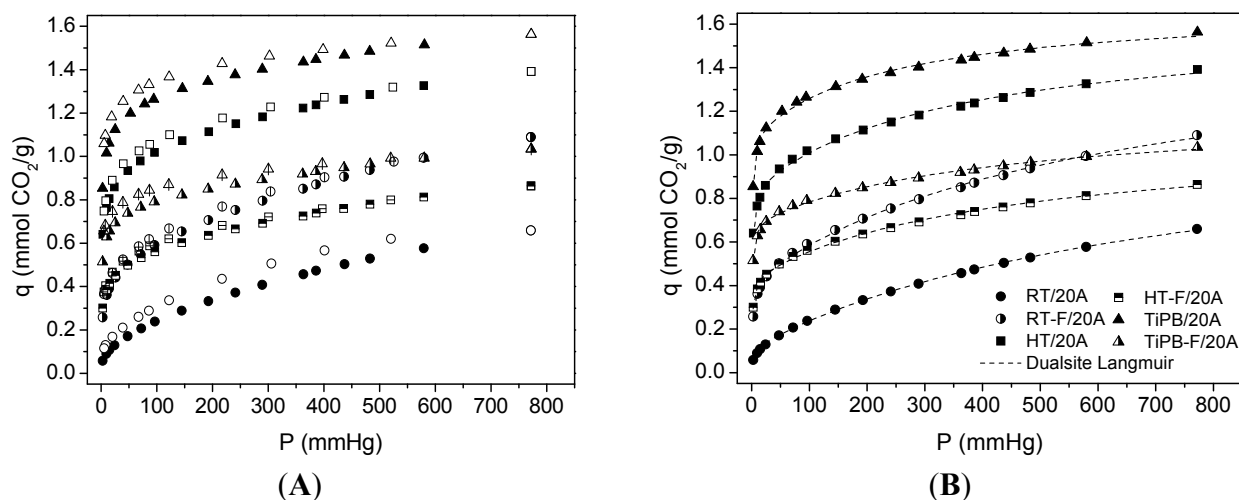


Figure 5. (A) CO₂ isotherms at 25 °C on 3-aminopropyltriethoxysilane (APTES)-grafted silicas. Adsorption data are the filled symbols and desorption data are the empty symbols; (B) dotted lines are fits from de Dualsite Langmuir model using adsorption data.

All CO₂ adsorption isotherms showed an initial steep slope at pressures below 100 mmHg, followed by a smooth increase in the amount of the adsorbed CO₂ from this pressure up. This behavior was also observed in impregnated silicas (see Figure 6). The nature of this steep rise can be related to the chemical reaction between CO₂ and amine groups, and the subsequent gradual increase in the amount of the adsorbed CO₂ attributed to CO₂ adsorbed by physisorption. In the case of high amine density, e.g., the impregnation with PEI, the CO₂ adsorbed interacts by hydrogen bonding with neighboring amine sites and promotes the formation of strongly adsorbed CO₂. This fact is confirmed by the high adsorption at lower absolute pressure. However, for low amine density, e.g., grafting with APTES, the CO₂ species lack neighboring amine sites and bind weakly adsorbed CO₂, so these sites can be easily removed; the chemisorptions sites of the materials functionalized with APTES are less strong than those functionalized with PEI [22,23]. From this reasoning and based on previous works [24,25], we used the Dualsite Langmuir model (DsL) (Equation (1)) to describe isotherms of functionalized materials with the aim to distinguish between the contributions due to chemical reaction and physical interactions.

$$q = \frac{q_1 K_1 P}{1 + K_1 P} + \frac{q_2 K_2 P}{1 + K_2 P} \quad (1)$$

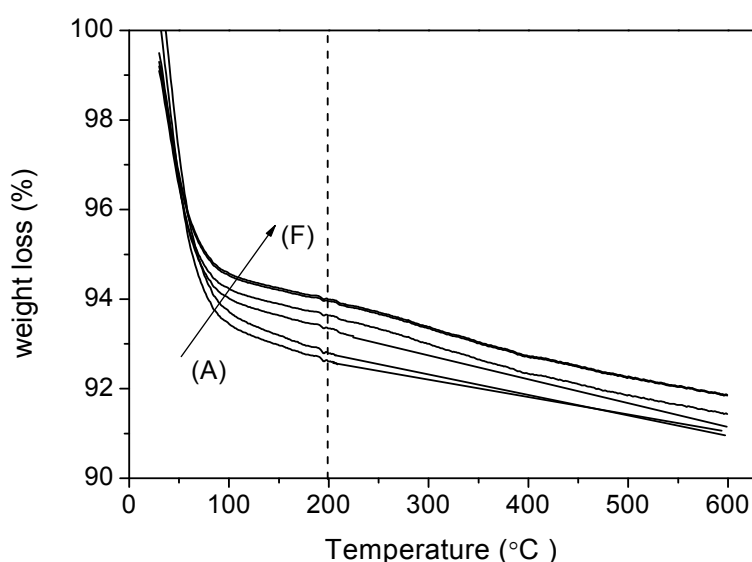


Figure 6. Thermogravimetry (TGA) thermograms of (A) RT; (B) RT-F; (C) HT; (D) HT-F; (E) TiPB and (F) TiPB-F.

Site 1 was taken as that with higher k parameter and is hence assigned as a chemisorption site whereas site 2 accounts for physical adsorption. The fitted parameters are presented in Table 4. It is noteworthy that the more ordered silicas showed higher CO₂ capacities than the pore expanded materials, in terms of physisorption (see q_2 values in Table 4), following the same trend observed in pure silicas. Despite the fact that the presence of a more extended microporous structure enhances physical adsorption of CO₂, the pore expanded materials show a higher amount of chemisorbed CO₂, because these materials have higher grafting yields, in agreement with elemental analysis results. APTES surface coverage [25,53], as calculated by Equation (2), is also included in Table 4.

$$\%APTES \text{ surface coverage} = \frac{\text{molar N content} \times 2 \times N_A}{3.7 \times S_{BET}} \times 100 \quad (2)$$

where N is the molar concentration of nitrogen (mol g^{-1}), as determined by elemental analysis, 2 accounts for the assumption that two surface silanol groups react with two ethoxy groups of each APTES molecule, in accordance with Chang *et al.* [54] who proposed bidentate coordination. S_{BET} is the BET surface area of amine-grafted silica (m^2g^{-1}) and 3.7 is the density of silanol groups per nm^2 , as determined by Shenderovich *et al.* [55] through Si-NMR analysis for this class of materials. Although not necessarily these materials present 3.7 as silanol density, for comparison purposes we can use that density as all materials synthesized in this work exhibit a similar silanol density. The silanol densities were estimated by thermogravimetry (TGA). In Figure 6, we can observe that the total weight losses of our pure adsorbents are in the range 8.1%–9.0%, consisting of two mass loss steps, below 200 °C attributed to the removal of the physically and the chemically adsorbed water and the weight loss above 200 °C is related to dehydroxylation by condensation of silanol groups. Due to the weight loss associated with the dehydroxylation being similar (around 2%) for all adsorbents, and from this value being related to the density of silanols [56], these results lead us to consider that the addition of swelling agents has only a slight effect on the silanol densities. However, solvent extraction as a template removal method could be an efficient method to increase this value [56].

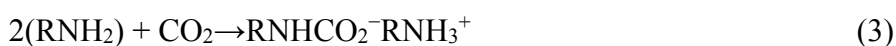
Table 4. Parameters from fit to Dualsite Langmuir model for amine grafting samples (20% APTES).

Sample	S_{BET}	%N	%APTES	Dualsite Langmuir model				q^*
				q_1	K_1	q_2	K_2	
RT	22	1.37	144	0.12 ± 0.01	0.247 ± 0.045	1.07 ± 0.03	$1.31 \times 10^{-3} \pm 9.95 \times 10^{-4}$	0.66
RT-F	102	2.85	65	0.43 ± 0.01	0.538 ± 0.071	1.17 ± 0.06	$1.65 \times 10^{-3} \pm 1.82 \times 10^{-4}$	1.09
HT	245	3.36	32	0.85 ± 0.01	0.984 ± 0.111	0.77 ± 0.04	$2.77 \times 10^{-3} \pm 3.89 \times 10^{-4}$	1.39
HT-F	260	2.41	21	0.44 ± 0.01	0.727 ± 0.079	0.66 ± 0.03	$2.25 \times 10^{-3} \pm 2.61 \times 10^{-4}$	0.86
TiPB	135	3.89	67	1.09 ± 0.02	1.449 ± 0.148	0.59 ± 0.02	$4.16 \times 10^{-3} \pm 6.22 \times 10^{-4}$	1.56
TiPB-F	198	2.70	32	0.69 ± 0.01	1.107 ± 0.099	0.52 ± 0.03	$2.30 \times 10^{-3} \pm 3.55 \times 10^{-4}$	1.03

Notes: S_{BET} : equivalent surface area, as determined by Brunauer-Emmett-Teller equation (m^2/g); %N: N content (wt%) as obtained by chemical elemental analysis (CNH); q_x : $\text{mmol CO}_2/\text{g}$; q^* : $\text{mmol CO}_2/\text{g}$ at 25 °C and 1 bar; K_x : mmHg^{-1} .

The %APTES values are summarized in Table 4. Note that the silanol density was fixed at 3.7 per nm^2 , which led to grafting yields over 100% (RT sample). It is likely that this sample contains a higher silanol density, above 3.7. However, only 1.37% N content was bonded on the RT sample surface. This could be due to the APTES molecules experiencing higher diffusional resistances through the narrow and long channels of the RT sample. This phenomenon is not expected to occur in less ordered materials, which explains the higher %N contents leading to higher CO_2 adsorption capacities.

In accord with previous works [27,57], primary and secondary amines (an APTES molecule has one primary amine) react with CO_2 through a zwitterion mechanism where water or amine group is needed (Equation (3))



Consequently, under our work conditions (dry conditions), two amine groups are required to capture one CO_2 molecule, so that the maximum CO_2/N adsorption efficiency is 0.5. Lower efficiencies may be

due to the lack of two amine groups sufficiently close to each other so as to allow reaction and formation of carbamate [58].

In addition, recently others authors have reported that the increase in CO₂ capture capacity of the N-containing materials could be also attributed to hydrogen bonding interactions between hydrogen atoms (from C-H and N-H) and CO₂ molecules [59,60], providing a new mechanism of the interaction between CO₂ and N-doped materials.

The best CO₂ capacity at 25 °C and 1 bar in this work was 1.56 mmol CO₂/g or 7 wt%, found in the case of the TPiB silica sample. This value is in the range of those reported by other authors [25,57,61].

Figure 7 shows adsorption/desorption CO₂ isotherms at 25 °C for impregnated silicas (50 wt% PEI). The presence of amine groups on the silicas surface, as observed in amine grafted silicas isotherms, causes a steep rise at low pressures. An outstanding CO₂ capacity is observed for the TiPB-F sample, reaching 1.87 mmol CO₂/g at 25 °C and 1 bar. All adsorption isotherms were fitted to the DsL model and the fit parameters are summarized in Table 5. For PEI impregnated silicas, we observed a gradual increase in both chemical and physical CO₂ adsorption (see q_1 and q_2 values and see also Figure 8). It seems that the evolution to the less ordered materials with expanded pores delays the pore blockage at higher PEI loadings. Further, the MCF type of arrangement improves the accessibility to amine groups, as we observed in previous works [24].

Upon loading of polyethylenimine up to a certain level, the porous structure of the original supports remained unchanged, although the surface area and pore volume decreased drastically. Accordingly, CO₂ adsorption capacities of the resulting adsorbents increased with the loading of PEI up to a maximum loading value, beyond which over-loading of the amines had a detrimental effect on CO₂ capture capacities.

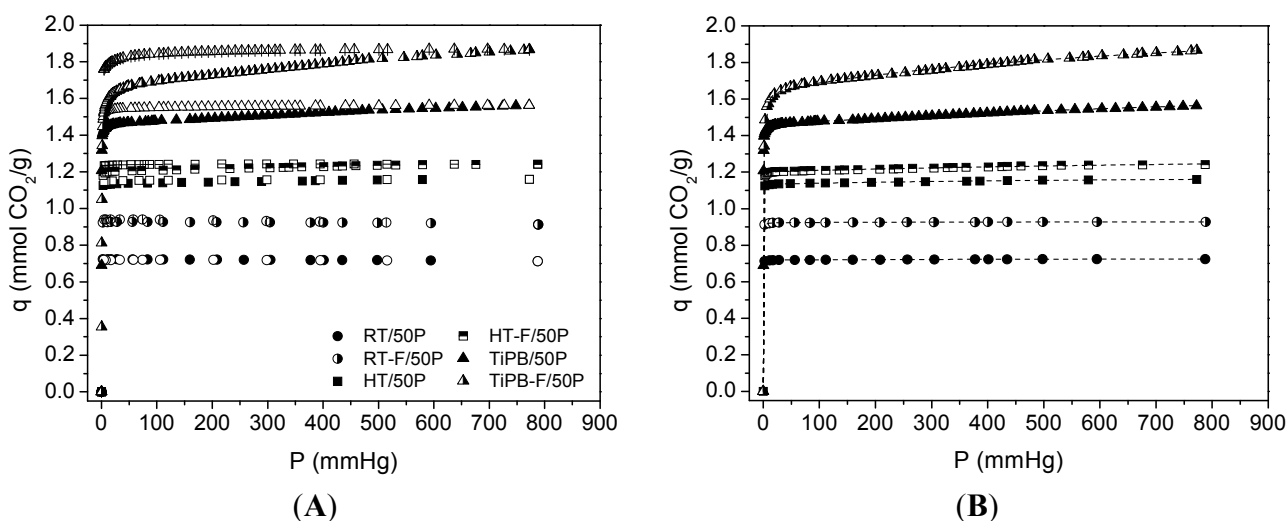
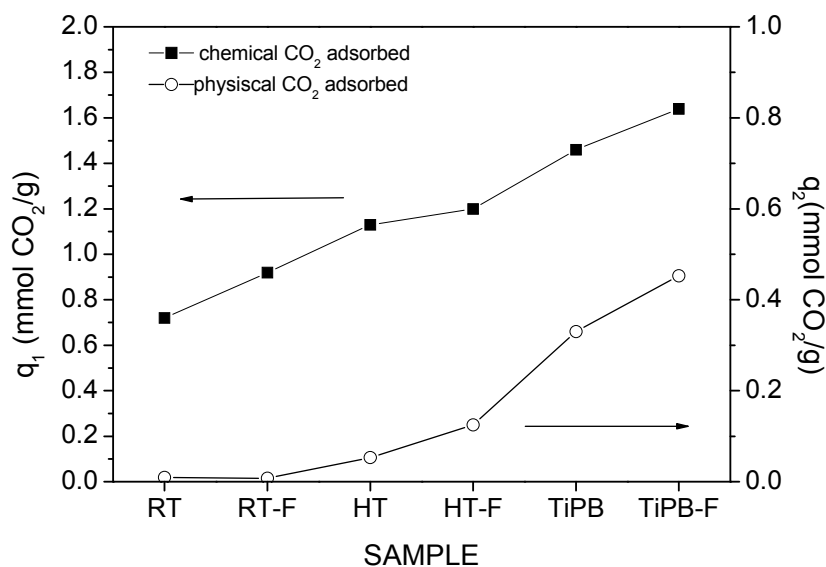


Figure 7. (A) CO₂ isotherms at 25 °C on polyethylenimine ethylenediamine branched (PEI)-impregnated silicas Adsorption data are the filled symbols and desorption data are the empty symbols; (B) dotted lines are fits from de Dualsite Langmuir model using adsorption data.

Table 5. Parameters from fit to Dualsite Langmuir model for amine impregnated samples (50% polyethylenimine ethylenediamine branched (PEI)).

Sample	S_{BET}	%N	Dualsite Langmuir model				q^*
			q_1	K_1	q_2	K_2	
RT	40	15.81	0.72 ± 0.01	56.051 ± 5.095	$9.21 \times 10^{-3} \pm 1.13 \times 10^{-3}$	$2.31 \times 10^{-3} \pm 7.40 \times 10^{-4}$	0.72
RT-F	81	15.07	0.92 ± 0.01	35.113 ± 2.874	$7.29 \times 10^{-3} \pm 1.91 \times 10^{-3}$	$2.33 \times 10^{-3} \pm 1.58 \times 10^{-3}$	0.93
HT	103	15.23	1.13 ± 0.01	42.840 ± 5.312	0.05 ± 0.01	$1.32 \times 10^{-3} \pm 2.64 \times 10^{-4}$	1.16
HT-F	101	14.18	1.20 ± 0.01	19.234 ± 1.299	0.12 ± 0.02	$6.53 \times 10^{-4} \pm 1.51 \times 10^{-4}$	1.24
TiPB	146	13.62	1.46 ± 0.01	11.783 ± 0.028	0.33 ± 0.03	$5.95 \times 10^{-4} \pm 7.19 \times 10^{-5}$	1.56
TiPB-F	171	14.63	1.64 ± 0.01	2.795 ± 0.069	0.45 ± 0.03	$1.12 \times 10^{-4} \pm 1.35 \times 10^{-5}$	1.87

Notes: S_{BET} : equivalent surface area, as determined by Brunauer-Emmett-Teller equation (m^2/g); %N: N content (wt%) as obtained by chemical elemental analysis (CNH); q_x : mmol CO_2/g ; q^* : mmol CO_2/g at 25 °C and 1 bar; K_x : $mmHg^{-1}$.

**Figure 8.** Evolution q_1 and q_2 PEI-silicas.

It is believed that under extreme high amine loadings, all the pores are filled and the external surface of SBA-15 will also be coated by the sticky amines, leading to limited accessibility of CO_2 towards the bulk amine molecules [62,63]. According to this reasoning, the maximum amount of amines that a mesoporous silica support can accommodate depends upon its pore volume. This hypothesis has been verified by experimental observation that when the volume corresponding to the amount of impregnated amine exceeds the total pore volume of the support, the resulting adsorbent appears to be sticky and gel-like. The high viscosity of the organic amines will also cause difficulties in CO_2 diffusion from the surface to the bulk amines, therefore a two-stage adsorption kinetics was observed (a fast surface reaction stage followed by a slower diffusion-controlling stage) [64,65], and where it appears that rather than lower temperatures, the highest capacities were typically obtained at 75 °C [52], so as to get rid of the diffusion barrier.

The sample that achieved the higher CO_2 capacity (TiPB-F/50 PEI) was also tested at 45 and 75 °C and CO_2 adsorption isotherms are shown in Figure 9. CO_2 capacity increases at higher temperatures, as expected. TiPB-F/50 PEI reached 1.87, 1.91 and 2.21 mmol CO_2/g at 25, 45 and 75 °C, respectively.

This increase in capacity at higher temperatures is due to chemisorption gain, as shown in Figure 10. The increase of the K_1 values (2.74, 3.25 and 4.61 mmHg⁻¹ for 25, 45 and 75 °C respectively) from DsL fit with temperature rise signifies that the process needs thermal energy, meaning that the process is endothermic. This is consistent with the assumption that chemisorptions occurs in site 1 [66]. SBA-15 synthesized from sodium silicate solution is a feasible option to obtain mesoporous silica with interesting capacities of CO₂ adsorption and probably with high CO₂/N₂ selectivity, especially SBA-15 impregnated and working at 75 °C, where the chemisorptions process prevails.

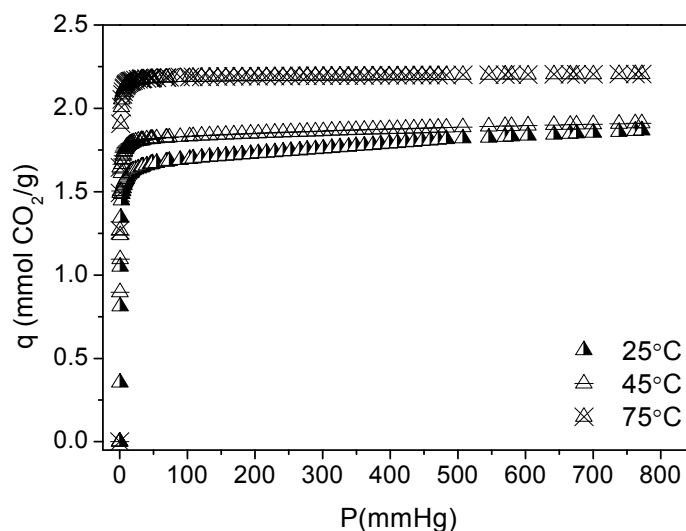


Figure 9. CO₂ adsorption isotherms for TiPB-F/50 PEI at 25, 45 and 75 °C.

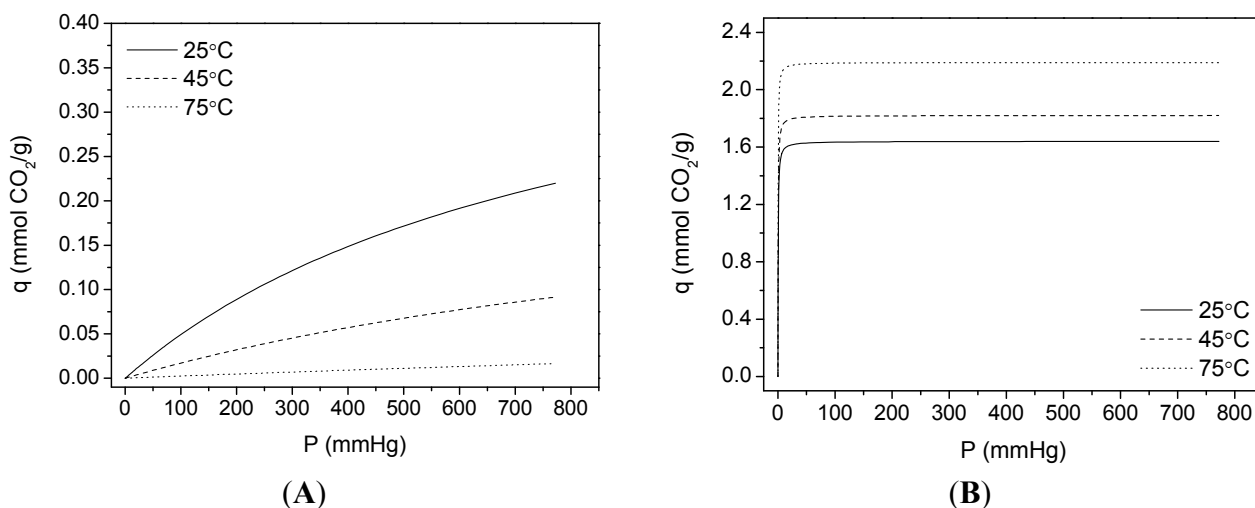


Figure 10. Deconvolution of CO₂ adsorption isotherms for TiPB-F/50PEI in their respective physisorption (A) and chemisorption (B) contributions.

4. Conclusions

Several mesoporous silicas were synthesized using sodium silicate, a cheaper silicon and environmentally benign source than traditional silicon alkoxides. The addition of swelling agents (1,3,5-triisopropylbenzene) and a solubility enhancer (ammonium fluoride) succeeded in producing materials with different textural features, but the addition of ammonium fluoride was not beneficial

because it led to materials with lower pore volume as compared to those from the same synthesis performed without ammonium fluoride.

The materials were functionalized by grafting with APTES (20% v/v) and by impregnation with PEI (50 wt%) and the CO₂ adsorption /desorption isotherms were measured. Materials with APTES had a direct relationship between the capacity and surface area of the non-functionalized material.

Among the materials synthesized, only SBA-15 synthesized at room temperatures (RT) improved its properties as an adsorbent with the addition of fluoride. The other solids showed poorer performance with the fluoride presence. The most promising result was the mesoporous silica synthesized with TIPB without fluoride (TIPB) at 25 °C and 1 bar CO₂ which captured 1.56 mmol/g (69 mg CO₂/g).

In the case of materials impregnated with PEI, the addition of fluoride was beneficial when synthesized with sodium silicate, the twisting up of the structure causes better performance of the material in terms of CO₂ adsorption, reaching 2.21 mmol CO₂/g at 75 °C and 1 bar. Therefore, compared with the results obtained in others works, sodium silicate can replace TEOS with the consequent reduction in the cost without the material losing potential properties as a CO₂ adsorbent.

Acknowledgments

The authors acknowledge financial support provided by the Spanish Ministry of Economy and Competitiveness CTQ2012-37925-C03-03 and FEDER funds, the Regional Government (Junta de Andalucía) P09-FQM-5070, the European Union Grant 295156, FP7-PEOPLE-2011-IRSES and Brazil-Spain Project PHB2011-0074-PC. E. Vilarrasa-García thanks to CAPES (Brazilian Ministry of Education) for fellowship.

Author Contributions

Enrique Vilarrasa García: This work was done as a part of his Ph.D. research; Juan Antonio Cecilia: He participated in the synthesis and characterization of the materials; Elisa M. Ortigosa Moya: She participated in the preparation of the porous solids; Celio L. Cavalcante Jr.: He participated in the adsorption measurements and in the discussion of the results; Diana C.S. Azavedo: She was co-advisor of the Ph.D. of Enrique Vilarrasa and participated in all the research; Enrique Rodríguez-Castellón: He was co-advisor of the Ph.D. of Enrique Vilarrasa and participated in all the research. The manuscript was written through contributions of all authors. All authors have given approval to the final version of the manuscript.

Conflicts of Interest

The authors declare no conflict of interest.

References

1. Houghton, J.T.; Ding, Y.; Griggs, D.J.; Noguer, M.; Linden, P.J.; Dai, X.; Maskell, K.; Johnson, C.A. *Climate Change: The Scientific Basis, Intergovernmental Panel on Climate Change*; The Press Syndicate of the University of Cambridge: Cambridge, UK, 2001.

2. Jacobson, M.Z. Review of solutions to global warming, air pollution, and energy security. *Energy Environ. Sci.* **2009**, *2*, 148–173.
3. Choi, S.; Drese, J.H.; Jones, C.W. Adsorbent materials for carbon dioxide capture from large anthropogenic point sources. *ChemSusChem* **2009**, *2*, 796–854.
4. Lee, S.Y.; Park, S.J. A review on solid adsorbents for carbon dioxide capture. *J. Ind. Eng. Chem.* **2015**, *23*, 1–11.
5. Song, C.-F.; Kitamura, Y.; Li, S.-H. Evaluation of Stirling cooler system for cryogenic CO₂ capture. *Appl. Energ.* **2012**, *98*, 491–501.
6. Rao, A.B.; Rubin, E.R. A technical, economic, and environmental assessment of amine-based CO₂ capture technology for power plant greenhouse gas control. *Environ. Sci. Technol.* **2002**, *36*, 4467–4475.
7. Favre, E. Membrane processes and postcombustion carbon dioxide capture: Challenges and prospects. *Chem. Eng. J.* **2011**, *171*, 782–793.
8. Olajire, A.A. CO₂ capture and separation technologies for end-of-pipe applications. A review. *Energy* **2010**, *35*, 2610–2628.
9. Oh, T.H. Carbon capture and storage potential in coal-fired plant in Malaysia: A review. *Renew. Sustain. Energy Rev.* **2010**, *14*, 2697–2709.
10. Zhang, J.; Singh, R.; Webley, P.A. Alkali and alkaline-earth cation exchanged chabazite zeolites for adsorption based CO₂ capture. *Micropor. Mesopor. Mater.* **2008**, *111*, 478–487.
11. Walton, K.S.; Abney, M.B.; LeVan, M.D. CO₂ adsorption in Y and X zeolites modified by alkali metal cation exchange. *Micropor. Mesopor. Mater.* **2006**, *91*, 78–84.
12. Cavenati, S.; Grande, C.A.; Rodrigues, A.E. Adsorption equilibrium of methane, carbon dioxide and nitrogen on zeolite 13X at high pressures. *J. Chem. Eng. Data* **2004**, *49*, 1095–1101.
13. Bai, B.C.; Cho, S.; Yu, H.-R.; Yi, K.-B.; Kim, K.-D.; Lee, Y.-S. Effects of aminated carbon molecular sieves on breakthrough curve behavior in CO₂/CH₄ separation. *J. Ind. Eng. Chem.* **2013**, *13*, 776–783.
14. Zhao, Y.; Zhao, L.; Yao, K.-X.; Yang, Y.; Zhang, Q.; Han, Y. Novel porous carbon materials with ultrahigh nitrogen contents for selective CO₂ capture. *J. Mater. Chem.* **2012**, *22*, 19726–19731.
15. Bao, Z.; Yu, L.; Ren, Q.; Lu, X.; Deng, S. Adsorption of CO₂ and CH₄ on a magnesium-based metal organic framework. *J. Colloid Interf. Sci.* **2011**, *353*, 549–556.
16. Millward, A.R.; Yaghi, O.M. Metal–Organic Frameworks with exceptionally high capacity for storage of carbon dioxide at room temperature. *J. Am. Chem. Soc.* **2005**, *127*, 17998–17999.
17. Sanz, R.; Calleja, G.; Arencibia, A.; Sanz-Pérez, E.S. CO₂ adsorption on branched polyethyleneimine-impregnated mesoporous silica SBA-15. *Appl. Surf. Sci.* **2010**, *256*, 5323–5328.
18. Khatri, R.A.; Chuang, S.S.C.; Soong, Y.; Gray, M. Thermal and chemical stability of regenerable solid amine sorbent for CO₂ capture. *Energy Fuels* **2006**, *20*, 1516–1520.
19. Yue, M.B.; Chun, Y.; Cao, Y.; Dong, X.; Zhu, J.H. CO₂ capture by as-prepared SBA15 with an occluded organic template. *Adv. Funct. Mater.* **2006**, *16*, 1717–1722.
20. Hiyoshi, N.; Yogo, K.; Yashima, T. Adsorption characteristics of carbon dioxide on organically functionalized SBA-15. *Micropor. Mesopor. Mater.* **2005**, *84*, 357–365.

21. Zelenak, V.; Badanicova, M.; Malanova, D.; Cejka, J.; Zukai, A.; Murafa, N.; Goerigk, G. Amine-modified ordered mesoporous silica. Effect of pore size on carbon dioxide capture. *Chem. Eng. J.* **2008**, *144*, 336–342.
22. Srikanth, C.S.; Chuang, S.S.C. Infrared study of strongly and weakly adsorbed CO₂ on fresh and oxidatively degraded amine sorbents. *J. Phys. Chem. C* **2013**, *117*, 9196–9205.
23. Tumuluri, U.; Isenberg, M.; Tan, C.-S.; Chuang, S.C. *In situ* infrared study of the effect of amine density on the nature of adsorbed CO₂ on amine-functionalized solid sorbents. *Langmuir* **2014**, *30*, 7405–7413.
24. Vilarrasa-García, E.; Ortigosa Moya, E.M.; Cecilia, J.A.; Cavalcante, C.L., Jr.; Jiménez-Jiménez, J.; Azevedo, D.C.S.; Rodríguez-Castellón, E. CO₂ adsorption on amine modified mesoporous silicas: Effect of the progressive disorder of the honeycomb arrangement. *Micropor. Mesopor. Mater.* **2015**, *209*, 172–183.
25. Vilarrasa-García, E.; Cecilia, J.A.; Santos, S.M.L.; Cavalcante, C.L., Jr.; Jiménez-Jiménez, J.; Azevedo, D.C.S.; Rodríguez-Castellón, E. CO₂ adsorption on APTES functionalized mesocellular foams obtained from mesoporous silicas. *Micropor. Mesopor. Mater.* **2014**, *187*, 125–134.
26. Harlick, P.J.E.; Sayari, A. Applications of pore-expanded mesoporous silica. Triamine grafted material with exceptional CO₂ dynamic and equilibrium adsorption performance. *Ind. Eng. Chem. Res.* **2007**, *46*, 446–458.
27. Mello, M.R.; Phanon, D.; Silveira, G.Q.; Llewellyn, P.L.; Ronconi, C.M. Amine-modified MCM-41 mesoporous silica for carbon dioxide capture. *Micropor. Mesopor. Mater.* **2011**, *143*, 174–179.
28. Builes, S.; Vega, L.F. Understanding CO₂ capture in amine-functionalized MCM-41 by molecular simulation. *J. Phys. Chem. C* **2012**, *116*, 3017–3024.
29. Heydari-Gorji, A.; Yang, Y.; Sayari, A. Effect of the pore length on CO₂ adsorption over amine-modified mesoporous silicas. *Energy Fuels* **2011**, *25*, 4206–4216.
30. Feng, X.; Hu, G.; Hu, X.; Xie, G.; Xie, Y.; Lu, J.; Luo, M. Tetraethylenepentamine-modified siliceous mesocellular foam (MCF) CO₂ capture. *Ind. Eng. Chem. Res.* **2013**, *52*, 4221–4228.
31. Fulvio, P.F.; Pikus, S.; Jaroniec, M. Short-time synthesis of SBA-15 using various silica sources. *J. Colloid Interf. Sci.* **2005**, *287*, 717–720.
32. Kruk, M.; Jaroniec, M.; Ko, C.H.; Ryoo, R. Characterization of the porous structure of SBA-15. *Chem. Mater.* **2000**, *12*, 1961–1968.
33. Zhang, H.; Sun, J.; Ma, D.; Bao, X.; Klein-Hoffmann, A.; Weinberg, G.; Su, D.; Schlögl, R. Unusual mesoporous SBA-15 with parallel channels running along the short axis. *J. Am. Chem. Soc.* **2004**, *126*, 7440–7441.
34. Kim, J.M.; Stucky, G.D. Synthesis of highly ordered mesoporous silica materials using sodium silicate and amphiphilic block copolymers. *Chem. Commun.* **2000**, *13*, 1159–1160.
35. Kassab, H.; Maksoud, M.; Aguado, S.; Pera-Titus, M.; Albela, B.; Bonneviot, L. Polyethylenimine covalently grafted on mesostructured porous silica for CO₂ capture. *RSC Adv.* **2012**, *2*, 2508–2516.
36. Gómez-Cazalilla, M.; Mérida-Robles, J.M.; Gurbani, A.; Rodríguez-Castellón, E.; Jiménez-López, A. Characterization and acidic properties of Al-SBA-15 materials prepared by post-synthesis alumination of a low-cost ordered mesoporous silica. *J. Solid State Chem.* **2007**, *180*, 1130–1140.

37. De Boer, J.H.; Lippens, B.C.; Linsen, J.C.P.; Broekhoff, J.C.P.; van den Heuvel, A.; Osinga, T.J. The t-curve of multimolecular N₂-adsorption. *J. Colloid Interf. Sci.* **1966**, *21*, 405–414.
38. Zhao, D.; Feng, J.; Huo, Q.; Melosh, N.; Fredrickson, G.H.; Chmelka, B.F.; Stucky, G.D. Triblock copolymer synthesis of mesoporous silica with periodic 50 to 300 angstrom pores. *Science* **1998**, *279*, 548–552.
39. Schmidt-Winkel, P.; Lukens, W.W., Jr.; Zhao, D.; Yang, P.; Chmelka, B.F.; Stucky, G.D. Mesocellular siliceous foams with uniformly sized cells and windows. *J. Am. Chem. Soc.* **1999**, *121*, 254–255.
40. Lettow, J.S.; Han, Y.J.; Schmidt-Winkel, P.; Yang, P.; Zhao, D.; Stucky, G.D.; Ying, J.Y. Hexagonal to mesocellular foam phase transition in polymer-templated mesoporous silicas. *Langmuir* **2000**, *16*, 8291–8295.
41. Miyazawa, K.; Inagaki, S. Control of the microporosity within the pore walls of ordered mesoporous silica SBA-15. *Chem. Commun.* **2000**, 2121–2122.
42. Imperor-Clerc, M.; Davidson, P.; Davidson, A. Existence of a microporous corona around the mesopores of silica-based SBA-15 materials templated by triblock copolymers. *J. Am. Chem. Soc.* **2000**, *122*, 11925–11933.
43. Galarneau, A.; Cambon, H.; di Renzo, F.; Fajula, F. True microporosity and surface area of mesoporous SBA-15 silicas as a function of synthesis temperature. *Langmuir* **2001**, *17*, 8328–8335.
44. Ravikovitch, P.I.; Neimark, A.V. Characterization of micro- and mesoporosity in SBA-15 materials from adsorption data by the NLDFT method. *J. Phys. Chem. B* **2001**, *105*, 6817–6823.
45. Luan, Z.; Fournier, J.A.; Wooten, J.B.; Miser, D.E. Preparation and characterization of (3-aminopropyl)triethoxysilane-modified mesoporous SBA-15 silica molecular sieves. *Microp. Mesop. Mater.* **2005**, *83*, 150–158.
46. Tanev, P.T.; Vlaev, L.T. An attempt at a more precise evaluation of the approach to mesopore size distribution calculations depending on the degree of pore blocking. *J. Colloid Interface Sci.* **1993**, *160*, 110–116.
47. Shen, S.C.; Kawi, S. Understanding of the effect of Al substitution on the hydrothermal stability of MCM-41. *J. Phys. Chem. B* **1999**, *103*, 8870–8876.
48. Kosslick, H.; Landmesser, H.; Fricke, R. Acidity of substituted MCM-41-type mesoporous silicates probed by ammonia. *J. Chem. Soc., Faraday Trans.* **1997**, *93*, 1849–1854.
49. Wang, X.; Schwartz, V.; Clark, J.C.; Ma, X.; Overbury, S.H.; Xu, X.; Song, C. Infrared study of CO₂ sorption over “Molecular Basket” sorbent consisting of polyethylenimine-modified mesoporous molecular sieve. *J. Phys. Chem. C* **2009**, *113*, 7260–7268.
50. Wang, X.G.; Lin, K.S.K.; Chen, J.C.C.; Cheng, S. Direct synthesis and catalytic applications of ordered large pore aminopropyl-functionalized SBA-15 mesoporous materials. *J. Phys. Chem. B* **2005**, *109*, 1763–1769.
51. Han, L.; Ruan, J.F.; Li, Y.S.; Terasaki, O.; Che, S.A. Synthesis and characterization of the amphoteric amino acid bifunctional mesoporous silica. *Chem. Mater.* **2007**, *19*, 2860–2867.
52. Heydary-Gorji, A.; Belmabkhout, Y.; Sayari, A. Polyethylenimine-impregnated mesoporous silica: Effect of amine loading and surface alkyl chains on CO₂ adsorption. *Langmuir* **2011**, *27*, 12411–12416.

53. Vilarrasa-García, E.; Cecilia, J.A.; Cavalcante, C.L., Jr.; Jiménez-Jiménez, J.; Azevedo, D.C.S.; Rodríguez-Castellón, E. Adsorción de CO₂ y separación CO₂/CH₄ en SBA-15 de poro expandido modificada con Ti y funcionalizada con APTES. *Mater. Adsorc. Catál.* **2014**, *7*, 30–47. (In Spanish)
54. Chang, F.Y.; Chao, K.J.; Cheng, H.H. Adsorption of CO₂ onto amine-grafted mesoporous Silicas. *Sep. Pur. Technol.* **2009**, *70*, 87–95.
55. Shenderovich, L.G.; Buntkowsky, G.; Schreiber, A.; Gedat, E.; Sharif, S.; Albrecht, J.; Golubev, N.S. Pyridine-¹⁵N a mobile NMR sensor for surface acidity and surface defects of mesoporous silica. *J. Phys. Chem. B* **2003**, *107*, 11924–11939.
56. Wang, L.; Yang, R.T. Increasing selective CO₂ adsorption on amine-grafted SBA-15 by increasing silanol density. *J. Phys. Chem. C* **2011**, *115*, 21264–21272.
57. Sayari, A.; Belmabkhout, Y. Stabilization of amine-containing CO₂ adsorbents: Dramatic effect of water vapor. *J. Am. Chem. Soc.* **2010**, *132*, 6312–6314.
58. Knofel, C.; Martin, C.; Hornebecq, V.; Llewellyn, P.L. Study of carbon dioxide adsorption on mesoporous aminopropylsilane-functionalized silica and Titania combining microcalorimetry and *in situ* infrared spectroscopy. *J. Phys. Chem. C* **2009**, *113*, 21726–21734.
59. Xing, W.; Liu, C.; Zhou, Z.; Zhang, L.; Zhou, J.; Zhuo, S.; Yan, Z.; Gao, H.; Wang, G.; Qiao, S.Z. Superior CO₂ uptake of N-doped activated carbon through hydrogen-bonding interaction. *Energy Environ. Sci.* **2012**, *5*, 7323–7327.
60. Bermúdez, J.M.; Dominguez, P.H.; Arenillas, A.; Cot, J.; Weber, J.; Luque, R. CO₂ separation and capture properties of porous carbonaceous materials from leather residues. *Materials* **2013**, *6*, 4641–4653.
61. Gray, M.L.; Soong, Y.; Champagne, K.J.; Pennline, H.; Baltrus, J.P.; Stevens, R.W. Improved immobilized carbon dioxide capture sorbents. *Fuel Process Technol.* **2005**, *86*, 1449–1455.
62. Xu, X.C.; Song, C.S.; Andresen, J.M.; Miller, B.G.; Scaroni, A.W. Preparation and characterization of novel CO₂ “molecular basket” adsorbents based on polymer-modified mesoporous molecular sieve MCM-41. *Micropor. Mesopor. Mater.* **2003**, *62*, 29–45.
63. Sun, N.; Tang, Z.; Wei, W.; Snape, C.E.; Sun, Y. Solid adsorbents for low temperature CO₂ capture with low energy penalties leading to more effective integrated solutions for power generation and industrial processes. *Front. Energy Res.* **2015**, doi:10.3389/fenrg.2015.00009.
64. Wang, X.X.; Song, C.S. Temperature-programmed desorption of CO₂ from polyethylenimine-loaded SBA-15 as molecular basket sorbents. *Catal. Today* **2012**, *194*, 44–52.
65. Chen, Z.H.; Deng, S.B.; Wei, H.R.; Wang, B.; Huang, J.; Yu, G. Polyethylenimine-impregnated resin for high CO₂ adsorption: An efficient adsorbent for CO₂ capture from simulated flue gas and ambient air. *ACS Appl. Mater. Inter.* **2013**, *5*, 6937–6945.
66. Yang, R.T. *Gas Separation by Adsorption Process*; Imperial College Press: London, UK, 1997; Volume 1.